

Effective Analysis of Ridged Circular Waveguides with a Curvilinear Frequency-Domain Finite-Difference Approach

A. Fanti, G. Montisci, G. Mazzarella, and G. A. Casula

Dipartimento di Ingegneria Elettrica ed Elettronica
University of Cagliari, 09123 Cagliari, Italy

alessandro.fanti@diee.unica.it, giorgiom@diee.unica.it, giuseppe.mazzarella@diee.unica.it,
a.casula@diee.unica.it

Abstract — We present a frequency domain finite difference approach in curvilinear coordinates to the computation of the modes of circular ridged waveguides. The use of a polar mesh allows to avoid staircase approximations of the boundary, providing a very effective and accurate procedure. The proposed approach has been assessed, both in terms of accuracy and effectiveness, against general-purpose software, namely CST Microwave Studio and Ansys HFSS, showing a significant reduction of the computational burden.

Index Terms — Finite difference frequency domain, ridged circular waveguides, and waveguide modes.

I. INTRODUCTION

Application of ridged circular waveguides (RCW) [1] can be found in many components like filters, matching networks, orthomode transducers, polarizers, and circulators that are widely used in satellite and terrestrial communication systems [2-6]. Low-cost design, small size, and optimum performance of these components are essential to satisfy today's stringent payload requirements. In the design of these components it is therefore important to characterize accurately the transition between the empty circular waveguide and the RCW section, as well as the interaction between subsequent discontinuities.

The most effective approach to such characterization is the use of the mode-matching (MM) [7], since its computational load is insensitive to the length of the waveguide sections. Moreover, MM accuracy is more or less constant

as the discontinuities spacing becomes smaller. To implement an MM analysis of those components, the knowledge of both eigenvalues and field distribution of waveguides modes are required. For a circular waveguide, the analytic computation of modes is the simplest, and most accurate, approach since the mode distribution can be expressed in terms of Bessel functions [8, 9], and the eigenvalues are the well-known zeroes of these functions.

For RCWs, various numerical techniques have been proposed in the past to compute the modes of single [3], double [1, 10-11], triple [12, 13], and quadruple-ridged [1, 14-16] circular waveguides with ridges of uniform thickness or ridges that are radially cut. All these methods require the ridges to be of equal radial and angular width, and equispaced along the guide circular boundary. The latter requirement cannot be easily relaxed, since those methods use a modal approach, and this limits their flexibility. There is also a technique that allows for the ridges to be of different radial and angular width [17, 18], but this method present one serious disadvantage. Actually, if the total angular width of the ridges becomes larger and larger, the final matrices become more and more ill-conditioned and a suitable adaptive process is required to find a compromise between accuracy and computational efficiency.

Of course, also general purpose EM programs can be used, but, respective of the approach (FDTD, FEM, FIT) they require a very fine mesh to reach the accuracy needed for use in filter design. In principle, frequency-domain finite-difference (FDFD) approach [19], i.e., the direct discretization of the eigenvalue problem, is the

simplest strategy, but, in its standard form, it is a very effective solution only for rectangular waveguides, since the boundary is perfectly fitted to the discretization grid. On the other hand, the standard FDFD requires, for generic curved structures, a staircase approximation of the boundary and its effectiveness (computational burden versus accuracy) is significantly lowered. A further drawback of the standard FDFD approach is the requirement of two different grids for TE and TM modes, justified with the different boundary conditions. This means that TE and TM modes are not known in the same sampling points. However, in many applications, e.g., mode matching or FDTD (using [20]), TE and TM modes needs to be considered together, and in the same points, which prevents standard FDFD results to be easily used.

Aim of this work is to devise an FDFD approach for RCWs, tailored to the structure, but as simple as the standard one in the formulation. Use of a suitable polar grid (which perfectly fits the waveguide boundary) allows to evaluate the RCW modes with the required accuracy using order of magnitude less points than the standard approach. By generalizing a solution already used in [21] for elliptic regular waveguide, and in [22] for rounded-end waveguides, our approach is able also to compute both TE and TM modes on the same set of sampling points. This strategy leads to a very effective computation of the modes eigenvalues, since the matrices resulting from the FDFD procedure are highly sparse. Moreover, the proposed approach is insensitive to the ratio between the area occupied by the ridges and the total cross-sectional area. The presented technique has been validated through comparison with CST Microwave Studio and Ansys HFSS, showing to be significantly more efficient.

II. DESCRIPTION OF THE FDFD PROCEDURE

Let us consider a ridged circular waveguide (see Fig. 1). Both TE and TM modes can be found [23] from a suitable scalar eigenfunction, solution of the Helmholtz equation,

$$\nabla_r^2 \phi + k_r^2 \phi = 0 \quad (1)$$

with the boundary conditions (BC)

$$\begin{aligned} \frac{\partial \phi}{\partial n} &= 0 \quad (TE \text{ modes}) \\ \phi &= 0 \quad (TM \text{ modes}) \end{aligned}, \quad (2)$$

at the boundary of the ridged waveguide. Both equation (1) and the BC (2) can be replaced by a discretized version looking for the eigenfunction values at a suitable set of sampling points, and therefore replacing derivatives with finite approximations. This transforms equation (1) into a matrix eigenvalue problem

$$\underline{A}\underline{\phi} = -k_r^2 \underline{\phi}, \quad (3)$$

whose eigenvectors contain the samples of the potential ϕ at the discretization nodes. The resulting matrix is sparse so a very effective computation is possible [24].

The set of sampling points forms a grid, whose geometry depends on the waveguide section, and which defines a set of cells partitioning the section itself. If the waveguide boundary consists of straight lines, parallel to the coordinate axes, the finite difference method can be applied on a cartesian grid [25, Fig. 28]. This grid defines also a partition of the waveguide surface into rectangular cells, which are rectangular and fill exactly the waveguide section. In this case, grid points are the vertices (or the centers, depending on the implementations) of a partition made of rectangular cells, which exactly fills the section. For every other waveguide, the section cannot be exactly partitioned using rectangular cells. Rather, a cartesian grid can only approximate this section [26, Fig. 3], and this leads to numerical errors (since an eigenvalue problem is quite ill-conditioned [27]).

In order to get an high accuracy, the best approach is to discretize the waveguide surface maintaining also the correct geometry of the boundary. So a discretization scheme based on a non-cartesian grid must be used, which matches exactly the waveguide boundary. Therefore, the discretization nodes must be at the intersections of a suitable framework, in which the waveguide boundary is a coordinate curve. In this way the waveguide section is exactly partitioned into discretization cells. In order to discretize the RCW we use a polar framework with coordinates (r, α) , the same one for both TE and TM modes, with a

regular spacing on the coordinate lines with step Δr , $\Delta\alpha$ (see Fig. 1). We have built this grid in such a way that furthest sampling points are not on the boundary, but at a distance $\Delta r/2$, $\Delta\alpha/2$, and we let $\phi_{nq} = \phi(n\Delta r, q\Delta\alpha)$ as sample values of $\phi(r, \alpha)$, so that the center is a sampling point.

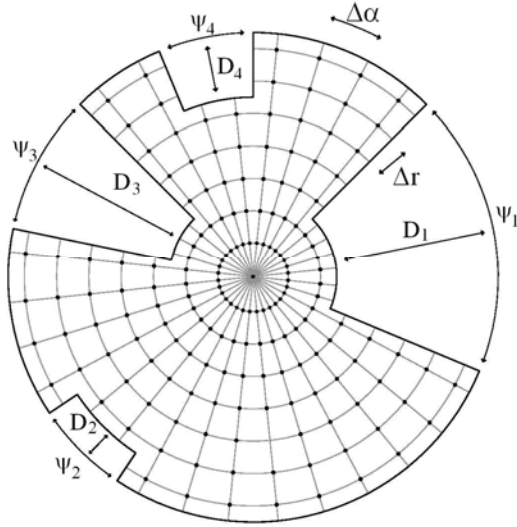


Fig. 1. An example of ridged circular waveguide with the curvilinear discretization grid.

We need a discretized version of equation (1) for each sampling point. For an internal point, such as P in Fig. 2, we start from the Helmholtz equation in polar coordinates,

$$\left[\frac{1}{r_p^2} \cdot \frac{\partial^2 \phi}{\partial \alpha^2} + \frac{1}{r_p} \cdot \frac{\partial \phi}{\partial r} + \frac{\partial^2 \phi}{\partial r^2} \right] = -k_t^2 \phi \quad (4)$$

and express the ϕ around the cell central point P using a second-order Taylor expression as,

$$\phi_D = \phi_P + \frac{\partial \phi}{\partial r} \Big|_P \cdot (\Delta r) + \frac{1}{2} \frac{\partial^2 \phi}{\partial r^2} \Big|_P \cdot (\Delta r)^2 \quad (5)$$

$$\phi_B = \phi_P + \frac{\partial \phi}{\partial r} \Big|_P \cdot (-\Delta r) + \frac{1}{2} \frac{\partial^2 \phi}{\partial r^2} \Big|_P \cdot (-\Delta r)^2. \quad (6)$$

Adding and subtracting equations (5) and (6) we get the derivatives in the r direction,

$$\begin{aligned} \frac{\partial^2 \phi}{\partial r^2} \Big|_P &= \frac{1}{\Delta r^2} \cdot (\phi_B + \phi_D - 2\phi_P) \\ \frac{\partial \phi}{\partial r} \Big|_P &= \frac{1}{2\Delta r} \cdot (\phi_D - \phi_B) \end{aligned} \quad (7)$$

and likely in α direction

$$\frac{\partial^2 \phi}{\partial \alpha^2} \Big|_P = \frac{1}{\Delta \alpha^2} \cdot (\phi_A + \phi_C - 2\phi_P). \quad (8)$$

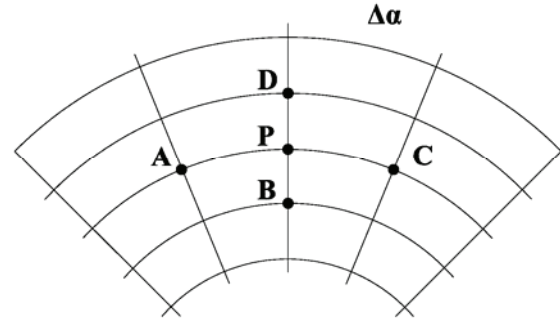


Fig. 2. Internal sampling point.

Now, inserting the derivatives of equations (7) and (8) into equation (4), we get its FD approximation,

$$\begin{aligned} \frac{\phi_A}{r_p^2 \Delta \alpha^2} + \left(\frac{1}{2r_p \Delta r} + \frac{1}{\Delta r^2} \right) \phi_D + \\ + \frac{\phi_C}{r_p^2 \Delta \alpha^2} + \left(\frac{1}{\Delta r^2} - \frac{1}{2r_p \Delta r} \right) \phi_B + \\ - \left(\frac{2}{\Delta r^2} + \frac{2}{r_p^2 \Delta \alpha^2} \right) \phi_P \cong -k_t^2 \phi_P^2 \end{aligned} \quad (9)$$

whose left hand side is the corresponding row of the matrix $\underline{\underline{A}}$ according to equation (3). However, equation (9) cannot be used:

- for the boundary points;
- for the center of the circle, which is a point of singularity for the polar frame;
- for the discretization points in the circle nearest to the center.

Therefore, all the above cases are treated separately in the following subsections.

A. Boundary points

Equation (9) cannot be used for boundary points, where BC of equation (2) must be enforced. In the polar grid used for a RCW, we have two types of boundary points: the radial ones (P in Fig. 3) and the angular ones (P in Fig. 4). The TE boundary condition can be enforced in the same way for both types of boundary points, so we describe it only for a radial one (Fig. 3). The boundary point X in Fig. 3 is not a discretization point. Therefore, the use of Taylor expansion

would require an extrapolation of $\phi(r)$ outside the sampling region, using either ϕ_X or ϕ_Y to enforce the boundary condition $\partial\phi/\partial n = 0$. Actually, we can use two different FD approximations for the normal derivative on the waveguide boundary,

$$\frac{\partial\phi}{\partial n}\Big|_X \simeq \frac{\phi_X - \phi_P}{\Delta r / 2}, \quad (10)$$

or

$$\frac{\partial\phi}{\partial n}\Big|_X \simeq \frac{\phi_Y - \phi_P}{\Delta r}. \quad (11)$$

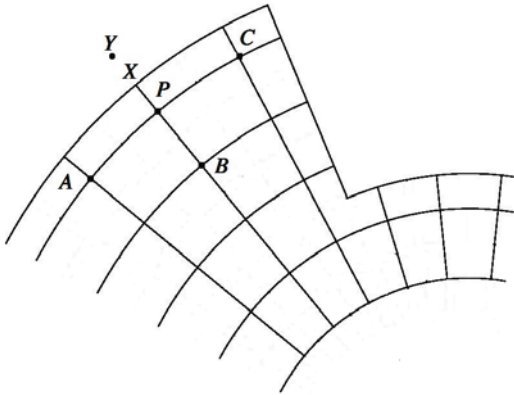


Fig. 3. Geometry pertinent to the first type of boundary point P .

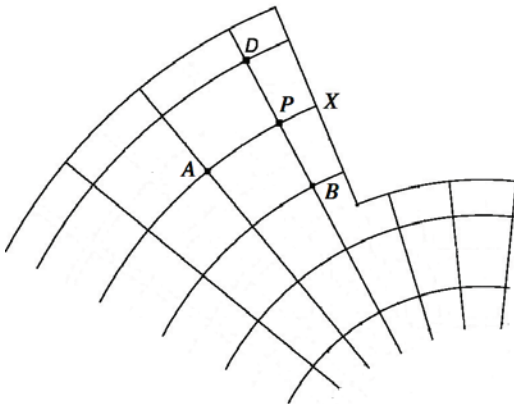


Fig. 4. Geometry pertinent to the second type of boundary point P .

The first one avoids an extrapolation outside the waveguide region, but has an error $O(\Delta r/2)$, whereas the second one is more accurate, with an error $O(\Delta r^2)$, but needs a ϕ value outside the waveguide. So we use the latter, to get $\phi_P = \phi_Y$. As a consequence, equation (7) is replaced by,

$$\begin{aligned} \frac{\partial^2\phi}{\partial r^2}\Big|_P &= \frac{1}{\Delta r^2} \cdot (\phi_B - \phi_P) \\ \frac{\partial\phi}{\partial r}\Big|_P &= -\frac{1}{\Delta r} \cdot (\phi_B - \phi_P) \end{aligned} \quad (12)$$

and equation (9) is replaced by,

$$\begin{aligned} \frac{\phi_A}{r_p^2\Delta\alpha^2} + \frac{\phi_C}{r_p^2\Delta\alpha^2} + \left(\frac{1}{\Delta\alpha^2} - \frac{1}{2r_p\Delta r}\right)\phi_B + \\ - \left(\frac{1}{\Delta r^2} - \frac{1}{2r_p\Delta r} + \frac{2}{r_p^2\Delta\alpha^2}\right)\phi_P \cong -k_i^2\phi_P^2 \end{aligned} \quad (13)$$

In the same way, for P in Fig. 4 we get,

$$\begin{aligned} \frac{\phi_A}{r_p^2\Delta\alpha^2} + \left(\frac{1}{2r_p\Delta r} + \frac{1}{\Delta r^2}\right)\phi_D + \\ + \left(\frac{1}{\Delta r^2} - \frac{1}{2r_p\Delta r}\right)\phi_B + \\ - \left(\frac{2}{\Delta r^2} + \frac{1}{r_p^2\Delta\alpha^2}\right)\phi_P \cong -k_i^2\phi_P^2 \end{aligned} \quad (14)$$

For the TM modes, we consider again the radial external point P (Fig. 3). Since, in this case, the BC of equation (2) require $\phi_X = 0$, we can express the potential in B and X using a Taylor approximation,

$$\begin{aligned} \phi_B &= \phi_P + \frac{\partial\phi}{\partial r}\Big|_P \cdot (-\Delta r) + \frac{1}{2} \frac{\partial^2\phi}{\partial r^2}\Big|_P \cdot (-\Delta r)^2 \\ \phi_X &= \phi_P + \frac{\partial\phi}{\partial r}\Big|_P \cdot \left(\frac{\Delta r}{2}\right) + \frac{1}{2} \frac{\partial^2\phi}{\partial r^2}\Big|_P \cdot \left(\frac{\Delta r}{2}\right)^2 \end{aligned} \quad (15)$$

Then, using equation (15) we get

$$\begin{aligned} \phi_B + 2\phi_X &= 3\phi_P + \frac{\partial^2\phi}{\partial r^2}\Big|_P \cdot \frac{3}{4}\Delta r^2 \\ \phi_B - 4\phi_X &= -3\phi_P - \frac{\partial\phi}{\partial r}\Big|_P \cdot 3\Delta r \end{aligned} \quad (16)$$

and, replacing the BC $\phi_X = 0$ in equation (16), we obtain the required derivatives in P ,

$$\begin{aligned} \frac{\partial^2\phi}{\partial r^2}\Big|_P &= \frac{4}{3\Delta r^2} \cdot (\phi_B - 3\phi_P) \\ \frac{\partial\phi}{\partial r}\Big|_P &= -\frac{1}{3\Delta r} \cdot (\phi_B + 3\phi_P) \end{aligned} \quad (17)$$

Finally, after substituting equations (17) and (8) into equation (4) we obtain,

$$\begin{aligned} & \frac{\phi_A}{r_p^2 \Delta \alpha^2} + \frac{\phi_C}{r_p^2 \Delta \alpha^2} + \\ & + \left(\frac{4}{3 \Delta r^2} - \frac{1}{3 r_p \Delta r} \right) \phi_B + \\ & - \left(\frac{4}{\Delta r^2} + \frac{1}{r_p \Delta r} + \frac{2}{r_p^2 \Delta \alpha^2} \right) \phi_P \cong -k_t^2 \phi_P^2 \end{aligned} \quad (18)$$

In the same way, for the point P in Fig. 4, equation (8) becomes,

$$\left. \frac{\partial^2 \phi}{\partial \alpha^2} \right|_P = \frac{4}{3 \Delta \alpha^2} \cdot (\phi_A - 3 \phi_P) \quad (19)$$

and, substituting equations (19) and (7) into equation (4), we get,

$$\begin{aligned} & \frac{4 \phi_A}{3 r_p^2 \Delta \alpha^2} + \left(\frac{1}{2 r_p \Delta r} + \frac{1}{\Delta r^2} \right) \phi_D + \\ & + \left(\frac{1}{\Delta r^2} - \frac{1}{2 r_p \Delta r} \right) \phi_B + \\ & - \left(\frac{2}{\Delta r^2} + \frac{4}{r_p^2 \Delta \alpha^2} \right) \phi_P \cong -k_t^2 \phi_P^2 \end{aligned} \quad (20)$$

B. Center of the circle

The center of the circle (P_0 in Fig. 5) is a point of singularity for the polar frame and no derivatives of ϕ can be computed there. As a consequence, it is not possible to use a Taylor expression using P_0 as initial point. The relevant equation is therefore obtained in a different way, by integrating equation (1) over a circle of radius $\Delta r/4$,

$$\int \nabla_t^2 \phi dS = -k_t^2 \int \phi dS. \quad (21)$$

Then, using the Gauss theorem on equation (21) we obtain,

$$\int_{\Gamma_F} \frac{\partial \phi}{\partial n} \cdot dl = -k_t^2 \int_{S_F} \phi dS \quad (22)$$

where in S_F is the cell surface, and Γ_F is the cell boundary (see Fig. 5).

The left hand side of equation (22) is then computed using the rectangular rule, with $N = 2\pi/\Delta\alpha$ steps. The relevant normal derivatives are computed using a first-order finite difference

approximation. The left hand side of equation (22) is therefore approximated by,

$$\sum_{q=1}^N \frac{(\phi_{A_q} - \phi_{P_0})}{\frac{\Delta r}{2}} \frac{\Delta r \Delta \alpha}{4}. \quad (23)$$

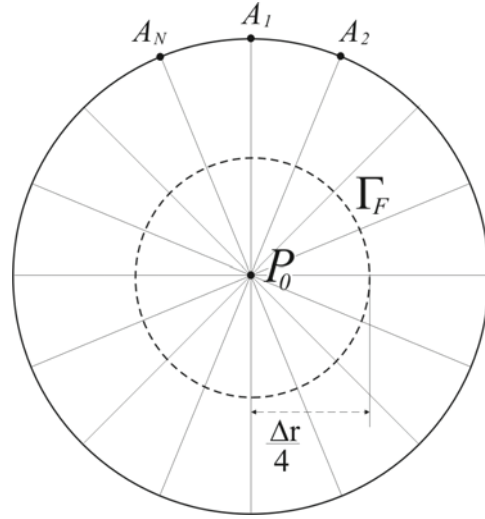


Fig. 5. Central point of the polar framework $|A_1 P_0| = \Delta r/2$.

The right hand side of equation (22) is likely computed as $-k_t^2 \phi_{P_0} \pi (\Delta r/4)^2$ and the discretized form of equation (1) in the center of the circle P_0 is

$$\left(\frac{1}{\pi \left(\frac{\Delta r}{4} \right)^2} \right) \sum_{q=1}^N \frac{(\phi_{A_q} - \phi_{P_0})}{\frac{\Delta r}{2}} \frac{\Delta r \Delta \alpha}{4} = -k_t^2 \phi_{P_0}. \quad (24)$$

C. Points in the circle nearest to the center

Finally, we are left to consider the internal points on the circle at distance $\Delta r/2$ from the center P_0 (see Fig. 6). For these points we can express the potential ϕ using a second order Taylor expression as,

$$\begin{aligned} \phi_D &= \phi_P + \left. \frac{\partial \phi}{\partial r} \right|_P (-\Delta r) + \left. \frac{1}{2} \frac{\partial^2 \phi}{\partial r^2} \right|_P \Delta r^2 \\ \phi_{P_0} &= \phi_P + \left. \frac{\partial \phi}{\partial r} \right|_P \left(\frac{\Delta r}{2} \right) + \left. \frac{1}{2} \frac{\partial^2 \phi}{\partial r^2} \right|_P \left(\frac{\Delta r}{2} \right)^2. \end{aligned} \quad (25)$$

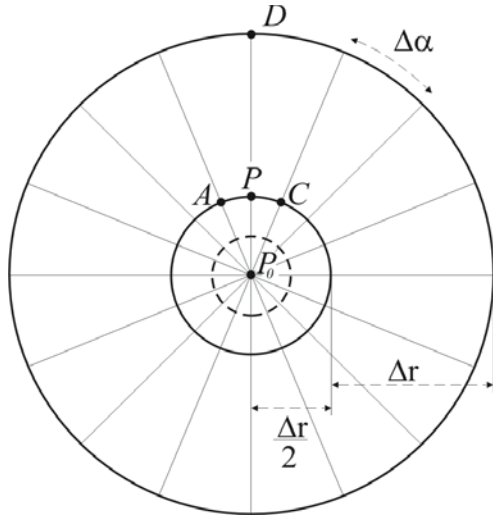


Fig. 6. Internal point P on the circle at distance $\Delta r/2$ from the center P_0 .

Then, we obtain

$$\begin{aligned} \phi_D + 2\phi_{P_0} &= 3\phi_P + \left. \frac{\partial^2 \phi}{\partial r^2} \right|_P \frac{3}{4} \Delta r^2, \\ \phi_D - 4\phi_{P_0} &= -3\phi_P - \left. \frac{\partial \phi}{\partial r} \right|_P 3\Delta r \end{aligned} \quad (26)$$

and the derivative in P is approximated by,

$$\begin{aligned} \left. \frac{\partial^2 \phi}{\partial r^2} \right|_P &= \frac{4}{3\Delta r^2} (\phi_D + 2\phi_{P_0} - 3\phi_P) \\ \left. \frac{\partial \phi}{\partial r} \right|_P &= -\frac{1}{3\Delta r} (\phi_D - 4\phi_{P_0} + 3\phi_P) \end{aligned} \quad (27)$$

After substituting equations (27) and (8) in to equation (4), we obtain

$$\begin{aligned} &\frac{\phi_A}{r_p^2 \Delta \alpha^2} + \left(\frac{4}{3\Delta r^2} - \frac{1}{3r_p \Delta r} \right) \phi_D + \\ &+ \frac{\phi_C}{r_p^2 \Delta \alpha^2} + \left(\frac{8}{3\Delta r^2} + \frac{4}{3r_p \Delta r} \right) \phi_{P_0} + \\ &- \left(\frac{4}{\Delta r^2} + \frac{1}{r_p \Delta r} + \frac{2}{r_p^2 \Delta \alpha^2} \right) \phi_P \cong -k_i^2 \phi_P^2 \end{aligned} \quad (28)$$

III. VALIDATION OF THE FDFD PROCEDURE

Since the cut-off frequencies scale as the inverse of the waveguide size, in all the

simulations presented in this section we will consider all dimensions (and Δr , too) normalized to the radius R of the circular waveguide. The FDFD procedure has been assessed against a commercial FIT software (CST Microwave Studio) and a FEM software (Ansys HFSS) both in terms of accuracy and effectiveness.

Since analytical eigenvalues are not available for RCWs with ridges of arbitrary dimension and position within the cross-sectional area, we have decided to test the accuracy and effectiveness of our procedure using a 270° sectorial waveguide, which is actually a limit case of the RCW described in Fig. 1 with a single ridge of dimension $D_1 = R$, and $\Psi_1 = 90^\circ$. This example has been chosen since it retains the more critical ridge feature, namely the convex wedge, which could affect the accuracy of numerical techniques. Therefore, the eigenvalues of the first five modes, computed either with the FDFD procedure or with CST and HFSS, have been compared with the analytical eigenvalues [28]. Actually, the FDFD procedure is able to reach (with a suitable discretization) a very high accuracy (see Tables I and II), so the true point to assess is its effectiveness. To do this, we have required, for both our FDFD, CST, and HFSS, that the amplitude of the relative error with respect to analytical eigenvalues is less than 0.1% or 0.02%. Then, we have investigated the computational resources needed by these simulations, which are summarized in Tables I and II. It is worth noting that both CST and HFSS require a minimum computational time which, for the computation of the first five eigenvalues, is respectively 48 sec and 14 sec, since the initial mesh is set automatically by these programs (these values are reported in bold characters in Tables I and II). In Figs. 7 and 8 the convergence behavior of the eigenvalue of the first TE mode (TE_1) and of the first TM mode (TM_1) is also shown. As apparent from Tables I and II, and Figs. 7 and 8, the computational time required by the FDFD procedure is significantly smaller than the one of CST Microwave Studio and Ansys HFSS (on a PC with 2 CPU Intel(R) Xeon(R) CPU E5504 @ 2.00 GHz, 8 core, Ram 48 GB).

Table I: Computational resources required to achieve a relative error less than 0.1 % with respect to analytical values.

Mode	Analytical Eigenvalue	FDFD			CST		HFSS		
		T [sec]	Sampling Points	Step ($\Delta\alpha$, Δr)	T [sec]	Tetrahedra	T [sec]	Tetrahedra	
TE ₁	1.4012180	0.8	27000	1°, 0.00995	53	10767	22	1465	Fig. 7
TE ₂	2.2577552	0.1	5400	1°, 0.04878	48	6143	14	1206	Not shown
TE ₃	3.0542369	0.1	5400	1°, 0.04878	48	6143	14	1206	Not shown
TM ₁	3.3756107	0.8	27000	1°, 0.00995	48	6143	26	1612	Fig. 8
TE ₄	3.8232239	0.1	5400	1°, 0.04878	48	6143	14	1206	Not shown

Table II: Computational resources required to achieve a relative error less than 0.02 % with respect to analytical values.

Mode	Analytical Eigenvalue	FDFD			CST		HFSS		
		T [sec]	Sampling Points	Step ($\Delta\alpha$, Δr)	T [sec]	Tetrahedra	T [sec]	Tetrahedra	
TE ₁	1.4012180	3.3	94500	1°, 0.00285	65	15584	163	5492	Fig. 7
TE ₂	2.2577552	0.2	9450	1°, 0.02817	48	6143	14	1206	Not shown
TE ₃	3.0542369	0.1	5400	1°, 0.04878	48	6143	14	1206	Not shown
TM ₁	3.3756107	3.8	108000	1°, 0.00250	53	10767	> 1000	> 20000	Fig. 8
TE ₄	3.8232239	0.1	5400	1°, 0.04878	48	6143	14	1206	Not shown

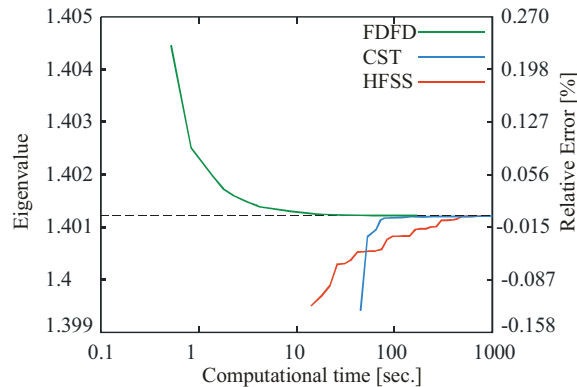


Fig. 7. Convergence behavior of the eigenvalue of the first TE mode. The dashed line represents the analytical value, and the relative error on the right is computed with respect to this value.

A further test to demonstrate the accuracy and effectiveness of the proposed FDFD procedure has been made using a circular waveguide with four ridges (see Fig. 9 and Table III). In this case, both a large ridge and very close and small ridges has been considered in order to assess the robustness of our procedure against a very dense mesh. Analytical results are not available for the structure in Fig. 9, therefore, in this case, our FDFD procedure has been assessed by comparison with the results of CST and HFSS. Due to the

particular geometry and relative position of the ridges #1, #2, and #3 in Fig. 9, a dense mesh is required and, therefore, the angular step of the FDFD grid has been selected equal to $\Delta\alpha = 0.25^\circ$, whereas the radial step Δr of FDFD and the mesh density of CST and HFSS have been varied to study the convergence.

In Fig. 10 the convergence behavior of FDFD compared to CST and HFSS is reported for a number of selected modes. Since all those programs use different discretization strategies, we have set the computational T time as independent variable. As apparent, the FDFD procedure is significantly faster than CST and HFSS, both for lower or higher order modes, either TE or TM. Further comments on Fig. 10 are in order. As a matter of fact, all programs considered have a hardware limit on the discretization size. This limit on CST (and also FDFD) depends on the required number of modes to be computed. For the structure in Fig. 9, we decided to solve the eigenvalue problem for the first 100 modes (61 TE and 39 TM). On the other hand, HFSS does not allow to compute more than 25 modes, so that its limit has been evaluated in this case. Moreover, both CST and HFSS have also a (quite large) minimum computational time since they set automatically the initial mesh. Table IV reports

both the minimum computational times and the computational times at the hardware limit, together with the corresponding meshes.

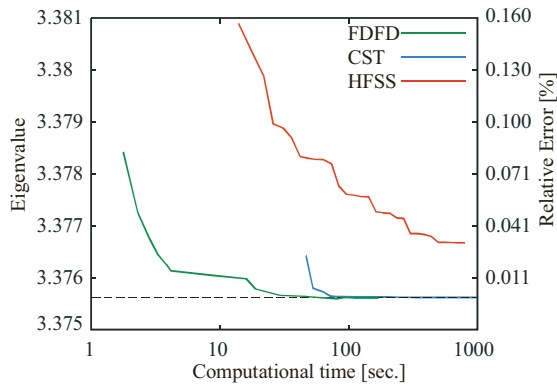


Fig. 8. Convergence behavior of the eigenvalue of the first TM mode. The dashed line represents the analytical value, and the relative error on the right is computed with respect to this value.

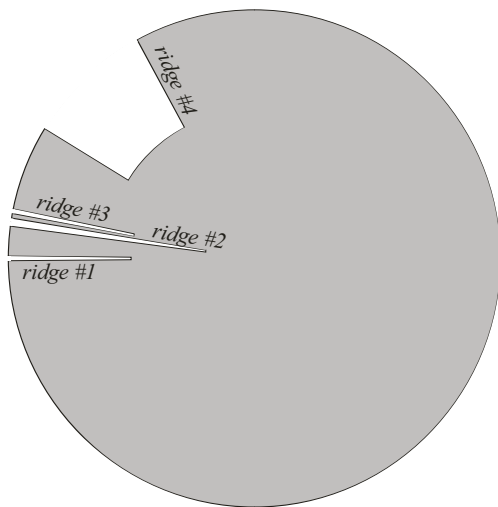


Fig. 9. Circular waveguide with four ridges. The geometry of the ridges is reported in Table III. Waveguide radius $R = 1$ (in normalized units). The angular spacing between ridge #1 and ridge #2 is 7° , between ridge #2 and ridge #3 is 1° , and between ridge #3 and ridge #4 is 20° .

Table III: Geometry of the ridges in Fig. 9.

Ridge	Radial width D_i	Angular width Ψ_i
#1	0.5	1°
#2	0.8	2°
#3	0.5	1°
#4	0.4	30°

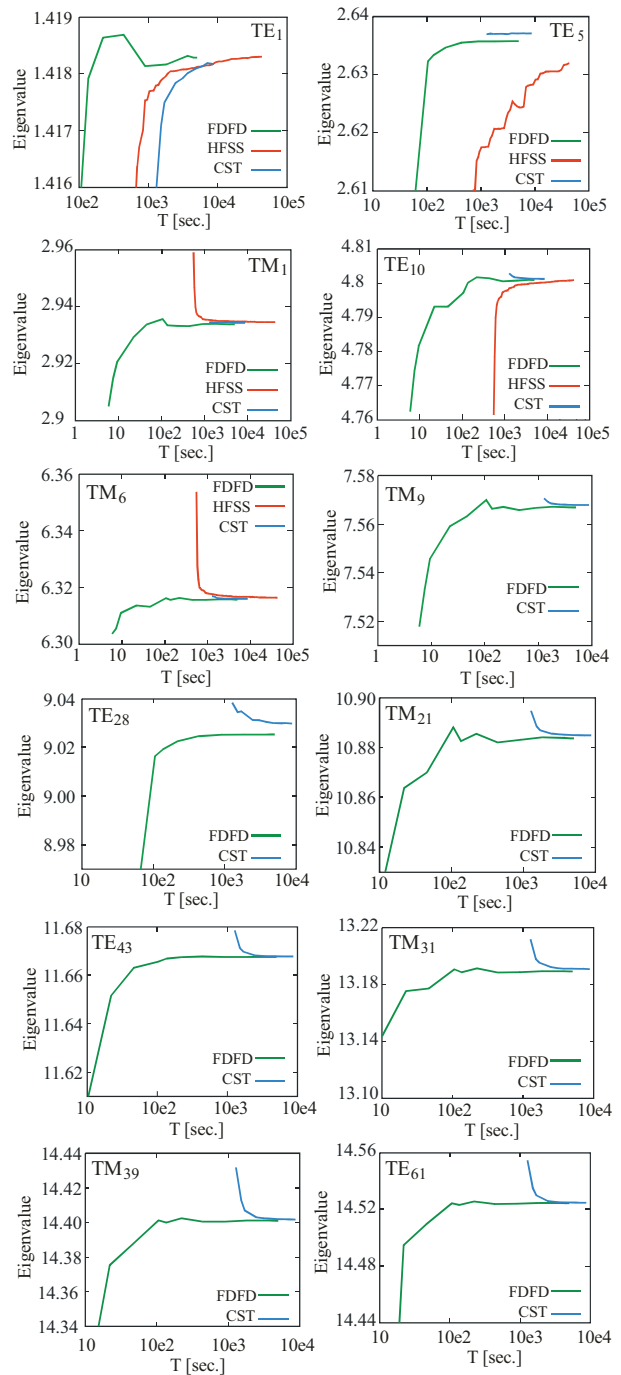


Fig. 10. Convergence behavior of the eigenvalues of selected TE and TM modes. The selected modes are reported with black dots in the curves in Fig. 11.

Table IV: Computational time (T) limits and mesh limits for the computation of the first 100 eigenvalues (either TE or TM) on a PC with 2 CPU Intel(R) Xeon(R) CPU E5504 @ 2.00 GHz, 8 core, Ram 48 GB.

	FDFD	CST	HFSS
Sampling Points at hardware limit	$10.3 \cdot 10^6$	-	-
Tetrahedra at hardware limit	-	501409	894798
T [sec] at hardware limit	5018	8760	43393
Initial mesh (Tetrahedra)	-	17701	9111
Minimum T [sec] (initial mesh)	-	1275	552

In Fig. 11, the relative difference of the eigenvalues computed with CST and HFSS with respect to those computed with the FDFD procedure is shown, using the densest available mesh (the one at the hardware limit, see Table IV). The comparison with HFSS is not complete because this software allows to compute a maximum of 25 modes (in this case 18 TE and 7 TM, since TE and TM are computed together). The results presented in Fig. 11, demonstrate the accuracy of our FDFD procedure both for TE and TM modes. Actually, the difference of the FDFD results with respect to HFSS is lower than 0.14 % (for the first 25 modes), whereas the difference with respect to CST results is lower than 0.05 % (for all the computed 100 modes).

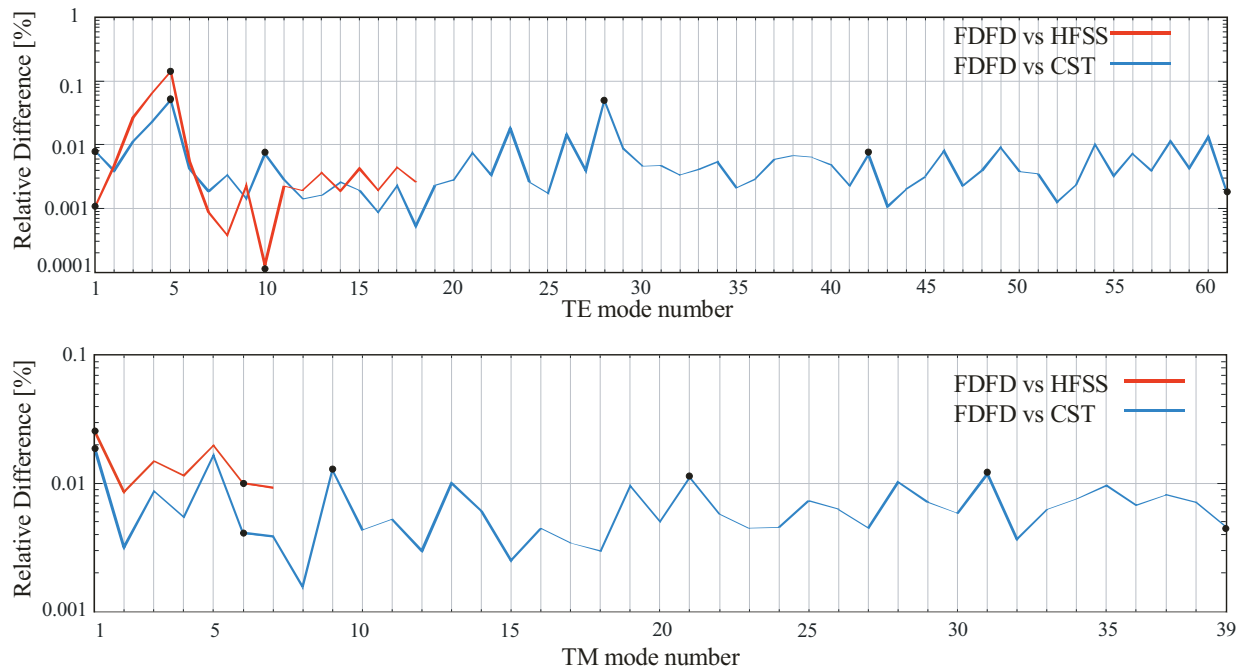


Fig. 11. Relative difference between the eigenvalues computed with the FDFD procedure and those computed with CST or HFSS, computed with the meshes reported in Table IV.

IV. CONCLUSION

We have proposed a finite difference approach to the computation of the modes of circular ridged waveguides. A polar mesh has been used in order to avoid staircase approximations of the boundary. The presented procedure allows to analyze a RCW, with an arbitrary number of ridges of arbitrary dimensions, with a computational burden and accuracy, which is independent both of the total cross-sectional area occupied by the ridges

and of the number of ridges. The proposed approach has been validated by comparison with the results of CST Microwave Studio and Ansys HFSS, showing a significant reduction of the computational time.

ACKNOWLEDGMENT

Alessandro Fanti gratefully acknowledges Sardinia Regional Government for the financial support of her Post Doctoral fellowship (P.O.R.

Sardegna F.S.E. Operational Programme of the Autonomous Region of Sardinia, European Social Fund 2007-2013 - Axis IV Human Resources, Objective 1.3, Line of Activity 1.3.1.).

REFERENCES

- [1] F. Canatan, "Cutoff wavenumbers of ridged circular waveguides via Ritz-Galerkin approach," *Electronic Letters*, vol. 25, pp. 1036-1038, Aug. 1989.
- [2] A. Williams and A. Atia, "Dual-mode canonical waveguide filters," *IEEE Transactions on Microwave Theory and Techniques*, vol. 25, no. 12, pp. 1021-1026, Dec. 1977.
- [3] R. Behe and P. Brachat, "Compact duplexer-polarizer with semicircular waveguide," *IEEE Trans. Antennas Propagat.*, vol. 39, pp. 1222-1224, Aug. 1991.
- [4] B. de la Filolie and R. Vahldieck, "Coaxial and circular waveguide band-pass filters using printed metal inserts," *IEEE MTT-S Int. Microwave Symp. Dig.*, pp. 905-908, 1992.
- [5] J. Huang, R. Vahldieck, and H. Jin, "Computer-aided design of circular ridged waveguide evanescent-mode bandpass filters using the FDTLM method," *IEEE MTT-S Int. Microwave Symp. Dig.*, pp. 459-462, 1993.
- [6] U. Balaji and R. Vahldieck, "Mode matching analysis of circular-ridged waveguide discontinuities," *IEEE Trans. Microwave Theory Tech.*, vol. 46, pp. 191-195, Feb. 1998.
- [7] A. Wexler, "Solution of waveguide discontinuities by modal analysis," *IEEE Trans. Microwave Theory and Techniques*, vol. 15, pp. 508-517, Sep. 1967.
- [8] R. Collin, *Foundations for Microwave Engineering*, 2nd Ed. New York: McGraw-Hill, Sect. 3.18, 1992.
- [9] M. Abramowitz and I. Stegun, *Handbook of Mathematical Functions*, (Applied Mathematics Series 55), Washington, DC: NBS, pp. 32-33, 1964.
- [10] D. Al-Mukhtar and J. Sitch, "Transmission-line matrix method with irregularly graded space," *IEE Proc.*, vol. 128, no. 6, pp. 209-305, Dec. 1981.
- [11] P. Daly, "Polar geometry waveguides by finite element methods," *IEEE Trans. Microwave Theory Tech.*, vol. 22, pp. 202-209, 1974.
- [12] B. Dillon and A. Gibson, "Triple-ridged circular waveguides," *Journal of Electromag. Waves Applicat.*, vol. 9, pp. 145-156, 1995.
- [13] A. Ornar, A. Jostingmeier, C. Rieckmann, and S. Lutgert, "Application of GSD technique to the analysis of slot-coupled waveguides," *IEEE Trans. Microwave Theory Tech.*, vol. 42, pp. 2139-2148, Nov. 1994.
- [14] Y. Tao, Z. Shen, and G. Liu, "Efficient analysis of quadruple corner-cut ridged circular waveguide by hybrid mode-matching boundary element method," *IEEE Trans. Magn.*, vol. 45, pp. 1076-1079, 2009.
- [15] M. Chen, N. Tsandoulas, and F. Willwerth, "Modal characteristics of quadruple-ridged circular and square waveguides," *IEEE Trans. Microwave Theory Tech.*, vol. 22, pp. 801-804, Aug. 1974.
- [16] W. Sun and C. Balanis, "Analysis and design of quadruple ridged waveguides," *IEEE Trans. Microwave Theory Tech.*, vol. 42, pp. 2201-2207, Dec. 1994.
- [17] S. Yu and J. Bornemann, "Classical eigenvalue mode spectrum analysis of multiple ridged rectangular and circular waveguides for the design of narrowband waveguide components," *Int. J. Numer. Model.*, vol. 22, pp. 395-410, April 2009.
- [18] S. Yu and J. Bornemann, "Evanescent-mode filters with arbitrarily positioned ridges in circular waveguide," *IEEE Pacific Rim Conference on Communications, Computers, and Signal Processing*, 2011.
- [19] K. Morton and D. Mayers, *Numerical Solution of Partial Differential Equations: An Introduction*, Cambridge University Press, Chapter 6, 2005.
- [20] F. Alimenti et al. "Efficient analysis of waveguide components by FDTD combined with time domain modal expansion," *IEEE Microw. Guided Wave Lett.*, vol. 5, pp. 351-353, Oct. 1995.
- [21] A. Fanti, G. Mazzarella, G. Montisci, and G. Casula, "Computation of the modes of elliptic waveguides with a curvilinear 2D frequency-domain finite-difference approach," *Progress In Electromagnetics Research M*, vol. 26, pp. 69-84, 2012.
- [22] A. Fanti and G. Mazzarella, "A finite difference polar-cartesian grid approach for mode computation in rounded-end waveguides," *ACES Journal*, vol. 26, no. 9, 2011.
- [23] O. Rübinkönig, *The Finite Difference Method (FDM) - An Introduction*, Albert Ludwigs, University of Freiburg, 2006.
- [24] G. Golub and C. Van Loan, *Matrix Computation*, Johns Hopkins University Press, 1989.
- [25] T. Itoh, *Numerical Techniques for Microwave and Millimeter-wave Passive Structures*, Chapter 2, Section 9.1, Wiley, New York, 1989.
- [26] J. Beggs and R. Luebbers, "Numerical analysis of staircasing effects on cutoff frequencies for FDTD modeling of circular waveguides," *Antennas and Propagation Society International Symposium. AP-S Digest*, pp. 547-549, 1993.

- [27] R. LeVeque, *Finite Difference Methods for Ordinary and Partial Differential Equations*, Philadelphia, PA: SIAM, Chapter 3, 2007.
- [28] R. Harrington, *Time-harmonic Electromagnetic Fields*, IEEE Press, John Wiley Interscience, New York, 2001.



Alessandro Fanti received the Laurea degree in Electronic Engineering and Ph.D. degree in Electronic Engineering and Computer Science from the University of Cagliari, Cagliari, Italy, in 2006 and 2012, respectively. He currently holds a

post-doc scholarship for design of microwave components. His research activity involves the use of numerical techniques for modes computation of guiding structures.



Giorgio Montisci received the Laurea degree (summa cum laude) in Electronic Engineering and Ph.D. degree in Electronic Engineering and Computer Science from the University of Cagliari, Cagliari, Italy, in 1997 and 2000, respectively. Since November

2000, he is Assistant Professor of electromagnetic field at the Dipartimento di Ingegneria Elettrica ed Elettronica, University of Cagliari, teaching courses in electromagnetics and microwave engineering. His research activity is mainly focused on analysis and design of waveguide slot arrays, microwave holographic techniques for the diagnostic of large reflector antennas, numerical methods in electromagnetics, and printed antennas. He is author or coauthor of about 40 papers in international journals and Reviewer for EM Journals.



Giuseppe Mazarella graduated Summa with Laude in Electronic Engineering from the Università "Federico II" of Naples in 1984 and obtained the Ph.D. in Electronic Engineering and Computer Science in 1989. In 1990, he became Assistant Professor at the

Dipartimento di Ingegneria Elettronica at the Università "Federico II" of Naples. Since 1992, he is with the Dipartimento di Ingegneria Elettrica ed Elettronica of the Università di Cagliari, first as Associate Professor and then, since 2000, as full Professor, teaching courses

in Electromagnetics, Microwave, Antennas and Remote Sensing. His research activity has focused mainly on: efficient synthesis of large arrays of slots, power synthesis of array factor, microwave holography techniques for the diagnostic of large reflector antennas, use of evolutionary programming for inverse problems solving. He is author (or co-author) of about 50 papers in international journals, and is a reviewer for many EM journals.



Giovanni Andrea Casula received the Laurea degree (summa cum laude) in Electronic Engineering and Ph.D. degree in Electronic Engineering and Computer Science from the Università di Cagliari, Cagliari, Italy, in 2000 and 2004, respectively. Since March 2006, he

is an Assistant Professor of electromagnetic field and microwave engineering at the Dipartimento di Ingegneria Elettrica ed Elettronica, University of Cagliari. His current research interests are in the field of synthesis, analysis and design of wire, patch, and slot antennas. Dr. Casula serves as reviewer for several international journals and is a member of the Italian Electromagnetic Society (SIEm).